

<https://doi.org/10.1038/s44355-024-00009-5>

# Impact of oxidized low-density lipoprotein on rat liver sinusoidal endothelial cell morphology and function

Check for updates

Hong Mao<sup>1,2,8</sup>, Larissa D. Kruse<sup>1,8</sup>, Ruomei Li<sup>1</sup>, Ana Oteiza<sup>3,4</sup>, Eike C. Struck<sup>5</sup>, Jasmin Schürstedt<sup>6</sup>, Wolfgang Hübner<sup>6</sup>, Victoria C. Cogger<sup>7</sup>, David Le Couteur<sup>7</sup>, Deanna L. Wolfson<sup>2</sup>, Thomas Huser<sup>6</sup>, Balpreet Singh Ahluwalia<sup>2</sup>, Cristina Øie<sup>1,9</sup> & Peter A. G. McCourt<sup>1,7,9</sup> ✉

Atherogenesis is associated with elevated plasma levels of oxidized low-density lipoproteins (oxLDL). In vivo, oxLDL causes liver endothelial swelling, and disrupts liver sinusoidal endothelial cell (LSECs) fenestrations. We mapped the nanoscale kinetics of these changes in vitro in isolated rat LSECs challenged with oxLDL and monitored viability with endocytosis and cytotoxicity assays. OxLDL disrupted LSEC ultrastructure – increasing oxLDL concentrations and oxidation levels caused sieve plate loss, fenestration fusion, and gap formation. Importantly, these effects were not uniform across all LSECs. LSECs retained the ability to endocytose ligands irrespective of the presence of oxLDL. However, increasing oxidation levels and concentrations of oxLDL inhibited LSEC mediated degradation of endocytosed ligands. Viability was unaffected by any oxLDL challenge. In conclusion, oxLDL disrupts LSEC ultrastructural morphology in vitro but LSECs remain viable and mostly maintain the scavenging function during oxLDL challenge.

Low-density lipoproteins (LDL) are the main carrier for the delivery of fat molecules (lipids, including cholesterol) in blood circulation via LDL receptor mediated endocytosis to peripheral tissues<sup>1</sup>, and elevated levels of LDL in the circulation are associated with the development of atherosclerosis<sup>2–5</sup>. Studies have pointed to the pathological role of oxidative modification of LDL in the development of these progressions, as non-modified LDL incubated with macrophages does not appear to elicit abnormal cholesterol accumulation<sup>6–8</sup>. LDL may transverse the endothelium at atherosclerotic sites, where they can be modified by oxidation or enzymatic activity, and taken up by macrophages and accumulate in atherosclerotic plaques<sup>9</sup>.

Oxidation of LDL can also occur in the plasma of healthy individuals<sup>10–14</sup>, and it can be oxidized in the arterial wall (during atherosclerosis) or in the circulating plasma<sup>10,13–15</sup>. The main form of circulating oxidized LDL (oxLDL) is mildly oxidized LDL, compared to the more heavily oxidized form of oxLDL found in the atherosclerotic plaques. Mildly

oxLDL was suggested to be the precursor of heavily oxLDL in the intima, and is a pathophysiological pro-atherogenic molecule in the body<sup>16,17</sup>. The level of oxidative modification of LDLs altered the properties of these molecules and their pathophysiological functions. Intravenously injected mildly oxLDL showed much slower liver uptake and had longer retention in circulation compared to heavily oxLDL, which may be sufficient to allow it to enter and accumulate in the arterial intima<sup>18</sup>. In addition to its key role in the development of atherosclerosis<sup>7,19–23</sup>, oxLDL is associated with the aging process as it is related to the pathogenesis of arterial stiffness, which is one of the main signs of vascular aging<sup>24</sup>. Endothelial thickening and reduced endocytosis are also signs of aging in LSEC<sup>25</sup> and can be the result of oxLDL exposure. Any change to porosity resulting from oxLDL as shown by Li et al. and Oteiza et al.<sup>25–27</sup> will affect clearance of lipoproteins from plasma.

Lipoprotein profile compositions are different in males and females. In various age groups, men are more likely to have lower high-density lipoprotein (HDL) than women and they generally have higher levels of LDL

<sup>1</sup>Vascular Biology Research Group, Department of Medical Biology, Faculty of Health Sciences, University of Tromsø -The Arctic University of Norway, Tromsø, Norway. <sup>2</sup>Optical Nanoscopy Research Group, Department of Physics and Technology, Faculty of Science and Technology, University of Tromsø -The Arctic University of Norway, Tromsø, Norway. <sup>3</sup>Nuclear Medicine and Radiation Biology Research Group, Department of Clinical Medicine, University of Tromsø -The Arctic University of Norway, Tromsø, Norway. <sup>4</sup>The PET Imaging Center, University Hospital of North Norway, Tromsø, Norway. <sup>5</sup>Translational Vascular Research Group, Department of Clinical Medicine, Faculty of Health Sciences, University of Tromsø -The Arctic University of Norway, Tromsø, Norway. <sup>6</sup>Bio-molecular Photonics, Faculty of Physics, Bielefeld University, Bielefeld, Germany. <sup>7</sup>ANZAC Research Institute, Concord Repatriation General Hospital, Concord, NSW, Australia; and The University of Sydney, Charles Perkins Centre, Nutritional Ecology and Physiology Lab, Sydney, NSW, Australia. <sup>8</sup>These authors contributed equally: Hong Mao, Larissa D. Kruse. <sup>9</sup>These authors jointly supervised this work: Cristina Øie, Peter A. G. McCourt. ✉e-mail: [peter.mccourt@uit.no](mailto:peter.mccourt@uit.no)

than women<sup>28</sup>. In total, atherosclerosis manifests differently in males and females, and the treatment of this disorder works differently between sexes<sup>28,29</sup>. Sex is often neglected as a variable in different types and areas of research, even though different studies show male and females are different (e.g. immune responses<sup>30</sup>, chronic pain<sup>31</sup>, cellular sex differences in the heart<sup>32</sup>). Therefore, in 2016 the US NIH published a “sex as a biological variable (SABV)” policy, emphasizing the inclusion of sex as a parameter in scientific and academic research and the European Commission also instructs researchers to include sex as a variable in their projects<sup>33,34</sup>. For this reason, the current study included male and female rodents.

Circulating oxLDL, as a major atherogenic substance<sup>10,35</sup>, is mainly removed from the blood by the cells lining the liver sinusoids<sup>36,37</sup>. Heavily oxLDL is taken up both by Kupffer cells and liver sinusoidal endothelial cells (LSECs)<sup>37</sup>, and mildly oxLDL is only recognized by LSECs<sup>27</sup>. This indicates that LSECs play an important role in eliminating plasma oxLDLs, demonstrating the importance of the liver cell clearance system in the prevention of cardiovascular disease<sup>12,38,39</sup>.

LSEC fenestrations (plasma membrane nanopores of 50–300 nm in diameter) regulate the size of lipoproteins entering the space of Disse where they are further metabolized by hepatocytes<sup>40,41</sup>. LSECs thus play a role in mediating the level of lipoproteins in the circulation, as defenestrated LSECs lead to the reduction of hepatic uptake of lipoproteins, which is one of the causes of hyperlipoproteinemia<sup>42</sup>. Similarly, the defenestration of LSECs is associated with the progression of non-alcoholic fatty liver disease (NAFLD), now termed metabolic dysfunction-associated steatotic liver disease (MASLD). Therefore, the dysfunction of LSECs in the early stages of NAFLD/MASLD might indicate the severity of subsequent progression of NAFLD/MASLD<sup>43,44</sup>.

Krüppel-like factor 2 (KLF2) is a transcription factor associated with vascular homeostasis, typically serving a protective role. Its downregulation is often a marker of endothelial dysfunction. It is an important regulator in endothelial cells (including LSEC) as it induces endothelial nitric oxide synthase (eNOS), which in turn regulates the production of nitric oxide (NO). This pathway supports endothelial function and vascular health through anti-inflammatory effects, vascular tone regulation and antithrombotic effects. KLF2 improves EC dysfunction and is accompanied by an increase in eNOS and phosphorylated eNOS. KLF2 is also reported to maintain LSEC morphology and it is considered a possible target for atherosclerotic vascular disease treatment (reviewed in<sup>45</sup>)<sup>46–48</sup>.

In addition to their bi-directional fenestration filter system, LSECs are well equipped with specific receptors for endocytosis, to fulfill their scavenger role in cleaning waste from the blood. For example, after intravenous administration of formaldehyde-treated serum albumin (FSA), it will distribute nearly exclusively to LSECs and be internalized via SR-H1/2 (also known as stabilin-1/2)-mediated endocytosis<sup>27,49,50</sup>. Therefore, FSA uptake in LSEC has been utilized as a functional biomarker for LSECs<sup>51,52</sup>. Of note, stabilin-1 and -2 also mediate the LSEC uptake of oxLDL, stabilin-1 and -2 having a higher affinity for mildly oxLDL and heavily oxLDL, respectively<sup>27</sup>. The downregulation of stabilin-1 and -2 has been shown in aging Wistar rats, while no reduction of those receptors could be observed in aging hybrid rats<sup>25,53</sup>. A reduction of the receptors stabilin-1 and -2 could lead to an increase in circulation time for oxLDL which could become more oxidized. However, there are multiple receptors that can take up oxLDL, which could compensate for the effect of reduced stabilin expression<sup>27</sup>.

In an *in vivo* study, oxLDL induced acute alterations in the liver microvasculature, such as narrowing of liver sinusoids, more swollen endothelial cells as well as endothelial thickening and reduced fenestration number<sup>26</sup>. These changes can lead to sinusoidal endothelial dysfunction.

Here, we report the *in vitro* effects of oxLDL on LSECs isolated from male and female rats, focusing on ultrastructural morphological alterations, using scanning electron microscopy (SEM) and fluorescence microscopy; and functionality using endocytosis studies in these cells.

## Results

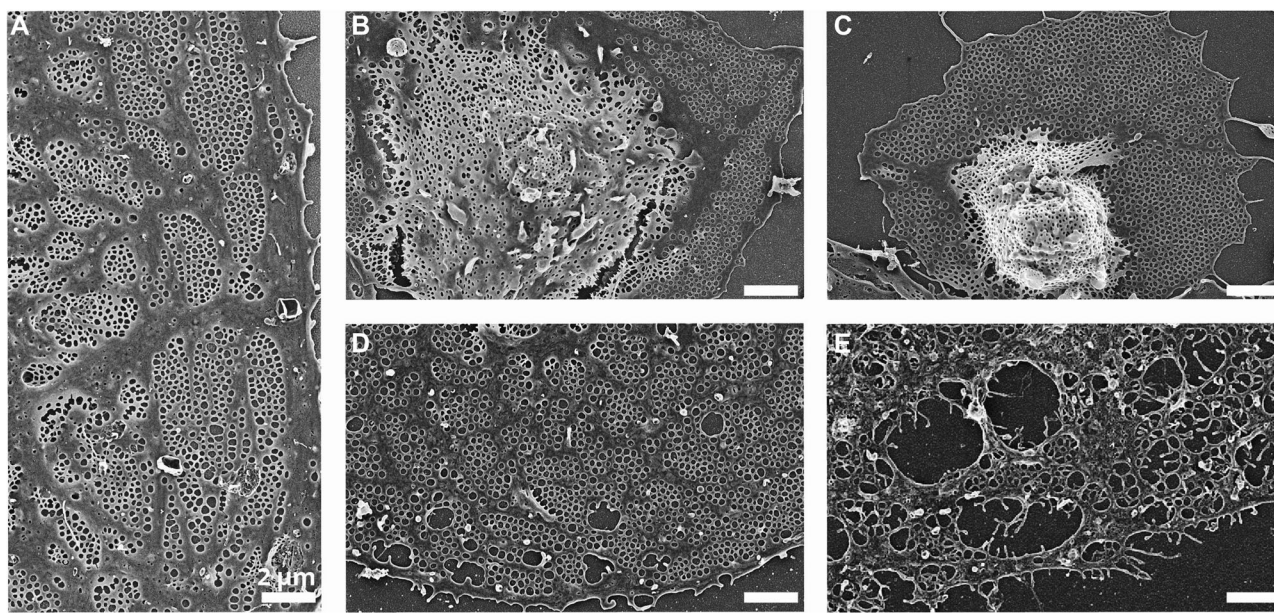
### Effects of oxLDL on cell morphology

SEM and SIM imaging were used to assess cultured LSEC fenestration alterations induced by various oxidation levels and doses of oxLDL (10, 40 and 80 µg/mL) in male and female rat cells (Figs. 1, 2). No obvious morphological gender differences were observed.

The effects of oxLDL on LSEC were not uniform within the same cell culture, with some LSECs appearing to be more resistant to oxLDL treatment, either mildly oxLDL (LDL oxidized with CuSO<sub>4</sub> for 3 h: oxLDL<sub>3</sub>) or heavily oxLDL (LDL oxidized with CuSO<sub>4</sub> for 24 h: oxLDL<sub>24</sub>). LSECs treated with 80 µg/mL oxLDL<sub>3/24</sub> induced loss of sieve plate organization (Fig. 1B, C), compared with control cells treated with RPMI cell medium only, which show typical distinct sieve plates with fenestrae (Fig. 1A). Despite the loss of organized sieve plates, the cell surface is still perforated with fenestrations. The loss of sieve plates seems to be more pronounced with higher LDL oxidation levels. Notably, in some cells there is a rather uniform distribution of the fenestrations throughout the entire cell surface in oxLDL<sub>24</sub> treated LSEC (Fig. 1C). On the other hand, the same concentration (80 µg/mL) oxLDL<sub>3/24</sub> can also lead to apparent fenestrae fusion and LSEC appearing with large trans-cytoplasmic gaps (Fig. 1D, E). The occurrence of such gaps was more pronounced with increasing oxidation levels of LDL. The same was observed with regard to cell finger-like membrane extensions (Fig. 1E). The higher the LDL oxidation and concentration, the more filaments/membrane remnants can be seen in the sample, likely resulting from the fused or broken fenestrations and membranes. Fenestration diameters were measured, and the results are shown under the micrographs in Fig. 1. In cells with sieve plate loss, oxLDL<sub>3/24</sub> challenge reduced the average fenestration diameter from 159 ± 38 nm (control) to 127 ± 38/126 ± 31 nm (oxLDL<sub>3/24</sub> respectively). In oxLDL<sub>3/24</sub> challenged cells with gaps, there was no change in fenestration diameter in oxLDL<sub>3</sub> treated cells, while in oxLDL<sub>24</sub> treated cells the average diameter was reduced to 101 ± 57 nm. In all treatments, fenestration diameters followed Gaussian distribution (supplementary information, figure S3).

Similarly, parallel to SEM samples, SIM microscopy was applied to monitor “wet” samples under the same oxLDL challenges to obviate the drying artifacts arising from SEM preparation, as well as to visualize the effects of oxLDL treatments on the same cell in real-time. Figure 2B shows that the higher LDL oxidation/concentration, the more fusions of fenestrations within the sieve plates were observed, leading to the formation of trans-cytoplasmic gaps of 2–4 µm in diameter, which can be seen in Fig. 2A. In general, the oxidation level of LDLs correlates with the fusion of fenestrations within sieve plates, i.e. higher oxidation levels of LDL cause more damage to LSEC morphology. Interestingly, oxLDL<sub>24</sub> in low doses (10 µg/mL) sometimes exhibits a unique combination of a fully fenestrated cell surface with scattered large gaps in between (Fig. 2A, oxLDL<sub>24</sub> 10 µg/mL). These fenestrations appear to be like those observed in the oxLDL<sub>24</sub> treated LSECs SEM image (Fig. 1C), which might have become large gaps in LSEC with a longer incubation time.

Live imaging shown in Fig. 2B provides in more detail the progress of large trans-cytoplasmic gap formations. Here, untreated LSECs (control) did not elicit major morphological changes over 30 min (20 time points) of laser exposure, although there was slight enlargement of some fenestrations (but not to the same degree as oxLDL treated cells). OxLDL<sub>3/24</sub> treated LSECs were imaged under the same photon load, indicating that any changes, such as trans-cytoplasmic gap formation, are not the result of any potential phototoxicity issues alone. Furthermore, we noted that “stand alone” small fenestrations tended to disappear (red dashed circles) with oxLDL challenge. During the oxLDL challenge, fenestrations tend to expand further and form large gaps by merging with smaller fenestrations within the same sieve plate (yellow dashed rectangles). From our observations, mildly oxLDL<sub>3</sub> elicited a slower response than oxLDL<sub>24</sub> on LSECs with regard to alterations in morphology. However, longer exposure to oxLDL<sub>3</sub> would likely elicit similar structural changes as the heavily oxLDL<sub>24</sub> does in the early stages.



Treatment		Fenestration Diameter [nm] ± SD	No. fenestrations counted	No. Gaps counted	Gap [%]
Oxidation levels of LDL	Concentration [µg/mL]				
SEM Control	-	159 ± 50	3846	192	4.75
OxLDL <sub>3</sub> (SP loss)	80	127 ± 38	2486	14	0.56
OxLDL <sub>24</sub> (SP loss)	80	126 ± 31	1753	12	0.68
OxLDL <sub>3</sub> (Gap)	80	166 ± 56	7203	339	4.49
OxLDL <sub>24</sub> (Gap)	80	101 ± 57	2110	456	17.77

**Fig. 1 | Representative scanning electron microscopy (SEM) images showing fenestration changes after treatment with LDL in different concentrations and degree of oxidation.** The images demonstrate the loss of sieve plates following treatment on male rat liver sinusoidal endothelial cells (LSECs). **A** Control LSEC SEM image showing typical fenestrations grouped in sieve plates. **B, C** 3/24 h copper sulfate-induced oxidized LDL (oxLDL<sub>3/24</sub>, 80 µg/mL, 30 min) treated LSEC SEM

images with increasing oxidation levels showing a pronounced loss of sieve plates and uniform fenestration distribution. **D, E:** oxLDL<sub>3/24</sub> (80 µg/mL, 30 min) treated LSEC SEM images with increasing oxidation levels showing the appearance of large trans-cytoplasmic gaps. Scale bar: 2 µm. Table shows analyzed fenestrations and gap data within cells with sieve plate loss (SP loss) or large gaps (Gap). The data were analyzed based on the representative figures above.

**Effects of oxLDL on the cytoskeleton**

Given that fenestrations within sieve plates are surrounded/supported by actin and tubulin, we performed fluorescence imaging (confocal and SIM) of the samples, staining for tubulin, actin and the membrane to determine what influence oxLDL has on the cytoskeleton of the cell. To test for any effects on endocytosis at the morphological level, we challenged the cultured LSEC with FSA-AF647. The distribution of endocytosed FSA-AF647 was more restricted to the perinuclear region in oxLDL treated cells compared to control cells.

In cells cultured in RPMI without treatment, a well-structured mesh of tubulin fibers can be seen (Fig. 3). In cells from both male and female rats, larger and smaller filaments are visible, while in the cells treated with 80 µg/mL of oxLDL<sub>24</sub> the tubulin fibers seem to be more condensed in certain areas with thicker fibers, leaving larger areas without tubulin. Those gaps can also be seen in the membrane staining, similar to those gaps visible in the SEM images (data not shown). Structured illumination microscopy (SIM) of the samples did not reveal any structural differences to single tubulin fibers (data not shown).

**Effects of oxLDL on cell viability and scavenger function**

To determine if oxLDL was directly toxic for LSEC, we performed viability (LDH release) (supplementary information, figure S1) and FSA endocytosis

scavenger function assays (Fig. 4) on cultured LSECs (male and female) that were challenged with oxLDL. The LDH assay showed a viability between 67% and 83% for male rat cells and 79%-83% for female rat cells (normalized to 0% viability under Triton X-100 treatment, which will cause 100% cell lysis without interfering with LDH activity), implying cells from females being slightly less affected than cells from males (supplementary information, figure S1; n (male/female) = 3).

The endocytic ability of LSECs following the challenge with oxLDL was tested by incubating the cells with <sup>125</sup>I-FSA. The endocytosis profiles (Fig. 4), from male and female rat cells, look similar. Statistical testing (Wilcoxon test) revealed no significant difference between the same treatments in male and female cells. Thus, for further statistical analyses (two-tailed, paired t-test), samples of the same treatment were grouped together (n = 6).

For both, male and female rats, at 10 µg/mL oxLDL concentrations, oxLDL<sub>3</sub> and oxLDL<sub>24</sub> did not significantly affect the endocytosis of <sup>125</sup>I-FSA, neither at the cell-associated nor the degradation level (supplementary information, figure S2). However, with increasing oxLDL concentrations and oxidation levels, components of endocytosis were significantly affected compared to endocytosis in the control group: the cell associated portion increased significantly in cells incubated with 40 µg/mL and 80 µg/mL of oxLDL<sub>3</sub>, as well as with oxLDL<sub>24</sub> at 80 µg/mL. In the cells treated with

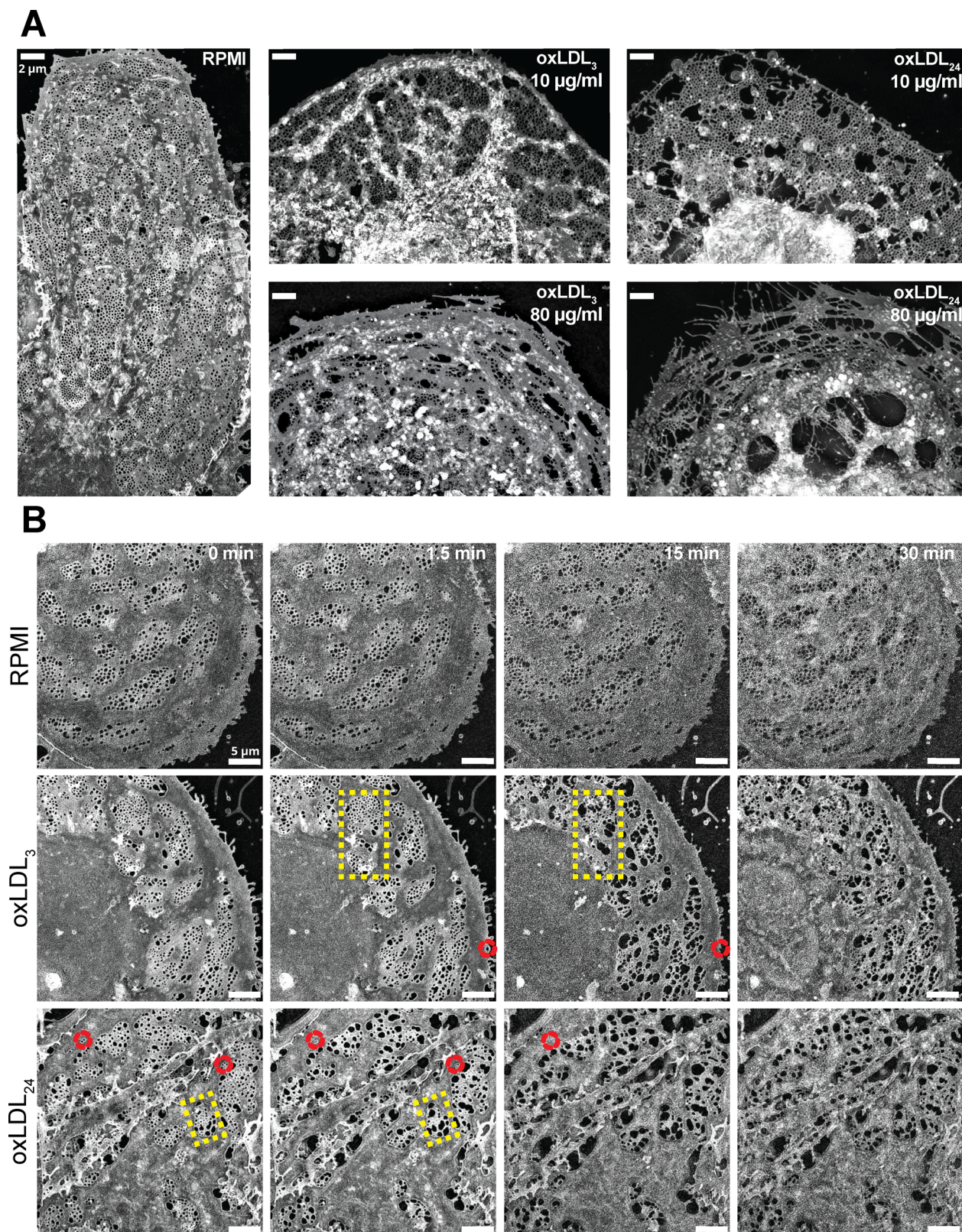


**Fig. 2 | Structured illumination microscopy (SIM) images of rat liver sinusoidal endothelial cells (LSECs) fenestration following treatments with LDL in different concentrations and degree of oxidation.** A SIM images on fixed LSECs stained with CellMask Green show the appearance of large trans-cytoplasmic gaps after 30 min of treatment with mildly and heavily oxidized LDL (10 µg/mL and 80 µg/mL). B Time-lapse images of live LSEC labeled with CellMask Green showing the effect of respective oxLDLs at 80 µg/mL. Fenestration changes occurred in real-time and

imaged every 1.5 min for 30 min (representative images at 0, 1.5, 15 and 30 min are shown): turning into large trans-cytoplasmic gaps for most of the fenestrations (yellow dashed rectangles) and disappearance of small fenestrations near the periphery (red dashed circle). The results are representative of experiments performed with 3 replicates. Images represent maximum intensity projections of a 1-2 µm 3D SIM z-stack and are individually intensity corrected for representation as the signal bleaches. Scale bar: 2 (A) and 5 (B) µm.

**Fig. 3 | Fluorescence microscopy of rat LSECs from male rats, comparing between cells cultured in RPMI only (control) and those treated with 80 µg/mL oxLDL<sub>24</sub>.** Upper row shows the merged channels stained for the cell nucleus (DAPI - blue), α-tubulin fibers (antibody against α-tubulin coupled to Alexa Fluor 488 - green), and the endocytosed FSA coupled to Alexa Fluor 647 (magenta). Pictures are representative of all imaged samples.

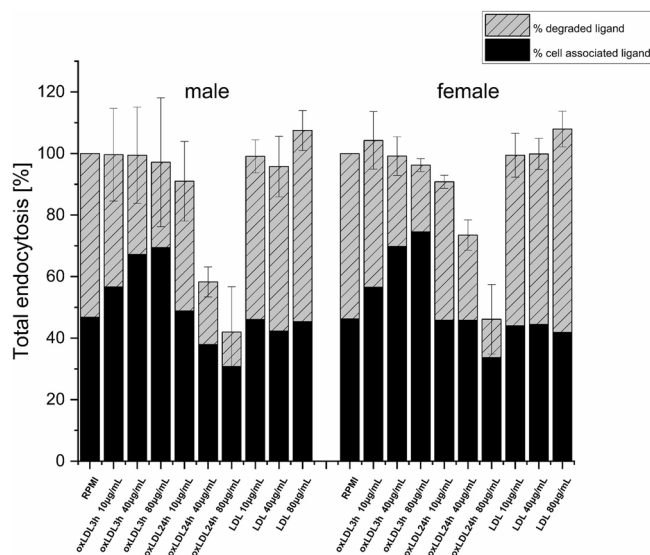
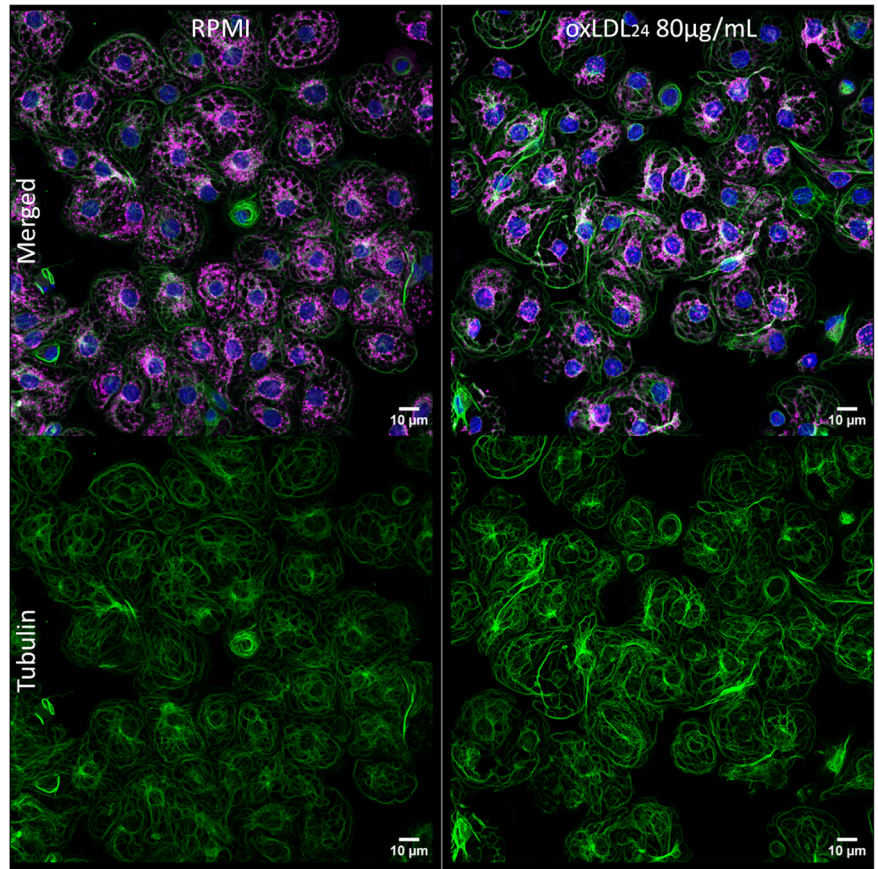


**Fig. 4 | Endocytosis of FSA bound to <sup>125</sup>Iodine in male and female rat LSECs preincubated with oxLDL in vitro.** Normalized to control (RPMI). Different doses (10/40/80 µg/mL) of oxLDLs treated LSEC cultures were incubated for 2 h at 37 °C with trace amounts of <sup>125</sup>I-FSA to assay for the main LSEC endocytosis receptors (stabilin1/2). Endocytosis was measured as described in Materials and Methods. Black bars represent cell-associated FSA (%CA), whereas the grey-striped bars represent degraded FSA (%DL). Total endocytosed radioactivity represents the sum of cell-associated and degraded ligand radioactivity, average of n = 3 animals per sex calculated.

oxLDL<sub>24</sub>, the effects seen were mainly as a reduction in <sup>125</sup>I-FSA degradation (statistically significant in all oxLDL<sub>24</sub>), with the effect being more pronounced with increasing concentrations of oxLDL<sub>24</sub>. The total endocytosis shows a step-like decline in the oxLDL<sub>24</sub> in male and female cells, but in comparison to the RPMI-only cultured cells, only the oxLDL<sub>24</sub> at concentrations of 40 µg/mL and 80 µg/mL have a significantly decreased effect on degradation.

LSEC maintain the capacity to take up FSA irrespective of the concentration and oxidation levels of oxLDL they are challenged with (also visually shown in Fig. 3), but at higher concentrations and oxidation levels of oxLDL, the intracellular degradation machinery in LSEC is negatively affected.

#### Effects of oxLDL on eNOS and KLF2 expression

KLF2 and eNOS are markers for vascular and endothelial health. The upregulation of KLF2 and eNOS is a reaction to and improves EC dysfunction<sup>46,48</sup>. The gene expression for both was analysed in different conditions. For KLF2, LDL treatment led to a significant downregulation, although 40 µg/ml and 80 µg/ml LDL treatments exhibit less downregulation compared to 10 µg/ml LDL exposure. Oxidation levels of LDL led to significant downregulation below half-fold for the mildly oxidized LDL, while the heavily oxLDL treatments reveal reduced or negligible effects (see Fig. 5). Gene expression analysis of eNOS for the same treatments shows no clear trend for any of the samples (supplementary information, figure S4).

Injury in LSECs may prompt variations in nitric oxide (NO) secretion, signifying alterations in vasodilatory signaling and endothelial health. To test whether oxLDL treatment induces changes in NO secretion, we performed the Griess assay using the supernatant of freshly isolated LSECs treated with LDL and oxLDL. The assay, even though a trend towards

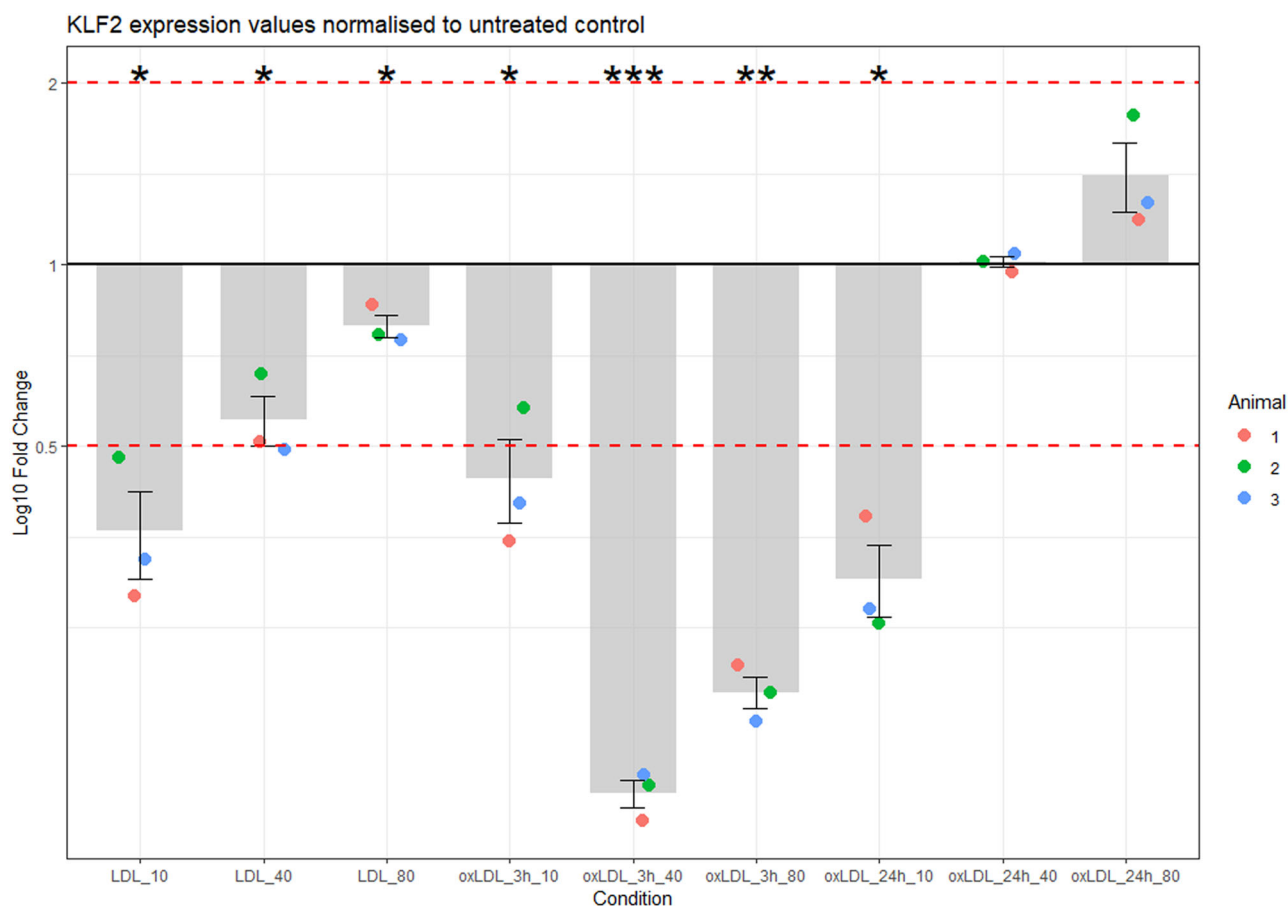


**Fig. 5 | Differential KLF2 gene expression in response to LDL and oxLDL treatments.** Fold change in KLF2 expression (log2) relative to untreated control across different conditions is shown. LDL treatments (10, 40, 80 µg/mL) and oxLDL treatments (3 h and 24 h oxidation at 10, 40 and 80 µg/mL) were analysed in three

rats. Error bars represent inter-animal variability. Statistical significance of treatment effects compared to control is indicated by asterisks (\*, \*\*, \*\*\*), where \* denotes  $p < 0.05$ , \*\* $p < 0.01$ , and \*\*\* $p < 0.001$ . Red dotted line represents 0.5- and 2-fold changes.

upregulation can be seen, does not show any significant changes in NO content in untreated versus LDL and oxLDL treated samples (see supplementary information, figure S5).

### Discussion

As a major atherogenic substance, oxLDL exists in atherosclerotic lesions and in the circulation<sup>10,35</sup>, and is mainly removed by cells lining in the liver sinusoids<sup>36,37</sup>. The liver is the main clearance organ for these heterogeneous particles, which may present as different forms in plasma<sup>26,54</sup>. As it already has pathogenic properties and is a physiological pro-atherogenic molecule, mildly oxLDL has been suggested to be the precursor of heavily oxLDL in the intima<sup>16,17</sup>, so its removal from the circulation by LSEC is beneficial for health. However, the effect that mildly (oxLDL<sub>3</sub>) or heavily (oxLDL<sub>24</sub>) oxidized LDLs have on LSECs at the cellular level has not been investigated. In our study, we tested their effects on LSECs isolated from female and male rats, with focus on ultrastructural morphological changes, using scanning electron microscopy (SEM) and structured illumination microscopy (SIM), and functionality using the ability of the cells to endocytose a model ligand (FSA). Given that there are differences in the lipoprotein profile between males and females, fine tuning of the concentrations might have revealed sex differences. However, no significant phenotypic nor functional differences were observed between male vs female results within our experimental setting, therefore the discussion is fused together for both sexes.

Oxidation of LDL for 20–24 h induces excessive modification (structural compositions, aggregation and fusion of molecules) of LDL<sup>55</sup>, which also increases the net negative charge relative to the complex compared to mildly oxLDLs<sup>27</sup>. Mildly oxLDL is the main circulating

form<sup>54</sup>, whereas heavily oxLDL is rarely detected in the circulation of healthy individuals<sup>35</sup>.

A previous in vivo study by Oteiza, et al.<sup>26</sup> showed that circulating oxLDL has significant negative effects on its clearance system, in that oxLDL challenged at clinically relevant plasma concentrations on mouse LSECs induced a reduction in the number of fenestrations. Our in vitro investigation on rat LSECs with physiologically relevant concentrations, shows negative effects, with more profound alterations on fenestrations (Figs. 1, 2): smaller fenestrations disappear or become smaller (supplementary information, figure S3), which is consistent with the in vivo finding<sup>26</sup>. With time, most turned into large trans-cytoplasmic gaps, which became more pronounced with increasing oxidation levels and concentrations of oxLDLs. Hence, the morphology of fenestrations in rat LSECs is clearly responsive to the oxLDL challenge. The mechanism of LSEC defenestration, however, remains to be determined.

Our SEM analysis demonstrated the loss of sieve plates post-oxLDL challenge (Fig. 1A), and this loss of sieve plates was apparent in previous in vivo findings but was not discussed by the authors<sup>26</sup>. Our SIM investigations showed effects of oxLDL<sub>24</sub> at low concentrations, characterized by loss of sieve plates and perforations with large trans-cytoplasmic gaps in a single cell after oxLDL<sub>24</sub> exposure at low concentrations (Fig. 2A oxLDL<sub>24</sub>, 10 µg/mL). This unique combination of both effects within one single cell might be a further stage after the loss of sieve plates shown in Fig. 1. The effects of oxLDL on LSECs were not uniform within the cells in the same cell culture, with some LSECs being more resistant to the oxLDL toxicity. While some cells demonstrated only the loss of sieve plates, Fig. 1B, C, and were covered by numerous fenestrations, in others, LSECs presented with large

trans-cytoplasmic gaps. Both effects were more profound with increasing oxidation levels of LDL.

The effect differences on LSEC might be due to the cells originating from different zones across the areas of liver lobules pre-perfusion (i.e. centrilobular and periportal regions), which show different morphological distributions of fenestrae. Vidal-Vanaclocha et al.<sup>56</sup> showed that clustered and free fenestrae distributed differently in the LSEC of these two regions. In addition, larger and higher numbers of fenestrae from centrilobular sinusoids with greater fenestrae size were reported in several studies<sup>52,56,57</sup>. Furthermore, a previous study showed that the oxLDL effects were most pronounced in LSECs from central liver lobule<sup>26</sup>. All these might explain why in our study the oxLDL effects were not uniformly observed on all cells. Further studies might be needed to understand the impact of oxLDL on LSECs from these two different liver zones.

Although SEM allows for high resolution imaging, SEM sample preparation procedures (e.g. dehydration) may induce artifacts such as alteration of drying artifacts and shrinkage of the specimen<sup>58</sup>. For instance, 15–30% shrinkage of the tissue was reported in SEM imaging when using the critical point drying step<sup>57</sup>. However, these induced artifacts can be avoided by using the SIM technique, which gives a resolution twice that of conventional light microscopy, and is sufficient to discern the average diameter (100 nm) of fenestrations on LSECs<sup>59</sup>. Furthermore, samples can be examined under wet conditions, i.e. the cells can be imaged under suitable culture conditions; therefore, fixation and dehydration are not absolute requirements, avoiding the generation of artifacts from dehydration; and a leading advantage of this technique is the potential for imaging living cells<sup>60,61</sup>.

Another consideration could be the stiffness of the cell substrate. Cells are seeded on glass or plastic, which are stiff materials compared to *in vivo* liver tissue. In a study from 2020, Guixé-Muntet et al. determined that the stiffness of the material influences the phenotype of LSECs, resulting in higher capillarization<sup>62</sup>. Thus, the possibility that the matrix on which the LSEC are seeded is partially responsible for changes in LSEC porosity, together with the oxLDL treatment, needs to be considered. However, since the control cells are also seeded on the same stiff matrix, the change in fenestration is most likely a result of the treatment.

Imaging the LSECs with SIM, we could observe the effects oxLDL (80 µg/mL) had on the cell membrane and fenestrations in real-time. To minimize photobleaching of our fluorophore, we imaged the cells 20 times during a 30 min time-period. Mildly oxLDL<sub>3</sub> in our *in vitro* findings elicited a slower response than heavily oxLDL<sub>24</sub> on LSECs with regard to changes in morphology. However, after a longer incubation time with oxLDL<sub>3</sub>, it will probably induce similar structural changes as the heavily oxLDL does at early stages. Thus, we suggest that mildly oxLDL with a longer circulatory life than the heavily oxLDL may have similar negative effects<sup>36,37</sup>, due to longer exposure time in contact with the vascular endothelial cells<sup>17,19</sup>. Therefore, effective LSEC clearance of circulating mildly oxLDL also is important in the prevention of cardiovascular disease<sup>12,38,39</sup>.

In addition to being a key component in atherosclerosis development, the modification of LDL turns it into a proinflammatory and cytotoxic substance<sup>8,23</sup>. KLF2 is associated with vascular homeostasis, its upregulation is often an indicator of endothelial dysfunction<sup>47</sup>. Mildly oxLDL causes downregulation of KLF2 in LSECs but – interestingly – heavily oxLDL does not elicit the same effect in this regard. The fact that mildly oxidized LDL (oxLDL) downregulates KLF2 in LSECs while heavily oxidized LDL does not, suggests that the extent of LDL oxidation may trigger distinct cellular pathways. Stabilin-1 has a greater affinity for mildly oxLDL than stabilin-2<sup>27</sup>, so it is therefore possible that this KLF2 down-regulation is mediated by stabilin-1 but not stabilin-2. This suggests a potential role for receptor-specific signaling in the regulation of KLF2, potentially making stabilin-1 a critical receptor in oxLDL-induced changes in endothelial function. However, given that LSECs express multiple oxLDL receptors, including scavenger receptors such as LOX-1 and CD36, the full picture likely involves complex interactions between these pathways, contributing to diverse outcomes based on the oxidation state of LDL.

In comparison to heavily oxLDL, the lower net negative charge of mildly oxLDL may have a low affinity for scavenger receptors, which may also explain the longer circulatory half-life, making it the predominant form present in human plasma<sup>27,63</sup>. Despite the presence of oxLDL in plasma<sup>27</sup>, and in this study, LSECs largely remain viable, and are able to function as scavenger cells, with effects on endocytosis and degradation only at high concentrations of oxLDL or high degrees of oxidation. The reason why mildly oxLDL has less effect on FSA degradation may be due to the lower receptor affinity for endocytosis of mildly oxLDL compared with heavily oxLDL. Heavily oxLDL was shown to be more efficiently taken up by LSECs<sup>27</sup>. Heavily oxLDL challenge of LSEC may thus induce more rapid disruptions of morphology and inhibition of intracellular degradation pathways. However, the inhibition of FSA degradation was more pronounced with increasing concentrations and oxidation levels of oxLDL in endocytosis studies (Fig. 4). Interestingly, LSEC maintained some ability to take up FSA, irrespective of the concentration or oxidation status of the oxLDL treatment. This would suggest that the early endocytic machinery continues to function as (essentially) normal, but subsequent steps in the endo-lysosomal pathway are affected by oxLDL.

Fluorescence microscopy confirms changes of the tubulin network in the cell. This was also not uniformly observed throughout the LSEC culture. As compared to control, non-treated cells, where the mesh of tubulin fibers is ubiquitous observed throughout the cytoplasm, in cells challenged with high concentration of oxLDLs or with high degree of oxidation, the tubulin network appears reduced, or condensed. Super resolution imaging showed no differences between the appearance of single tubulin fibers between the treatments, further confirming that oxLDL does not induce breakage or conformational changes to the tubulin fibers. The condensed fibers are rather the result of membranes pulling together when large gaps occur due to the treatment. Since the transport of internalized ligands to the lysosomes is microtubule-dependent<sup>64</sup>, our results using heavily oxLDL<sub>24</sub> at high concentration suggest that reduced degradation is due to disruption of the tubulin fiber network. Interestingly, Mönkemöller et al. 2015 showed that tubulin demarcated LSEC sieve plates, so oxLDL-mediated disruption of the tubulin network may also have implications for LSEC disruption/defenestration reported here<sup>65</sup>.

Another possibility that could contribute to the reduction in degradation is that heavily oxidized LDL, with all its chemical modifications, causes lysosomal “indigestion” due to enzyme changes in the lysosome<sup>66</sup> and thus renders the lysosome less able to degrade other substrates as well (such as FSA). Interestingly, the mildly oxLDL at higher concentrations only affected the degradation of FSA, while heavily oxLDL affected both degradation and cell associated fraction of FSA. Previous studies have shown that heavily oxLDL, as well as FSA, are taken up by the same receptor (stabilin 2), while oxLDL<sub>3</sub> is mainly taken up by stabilin 1<sup>27</sup>. Thus, the effect seen with heavily oxLDL may also be due to receptor competition for the same binding sites.

Notably, the dramatic *in vitro* effects on LSECs morphology via oxLDLs do not take into account the other cell types (hepatocytes, Kupffer cells) in the liver, and the mutual effects these cells will have on each other. The same cell types might be less (or more) affected *in vivo*. Co-cultures with multiple liver cell-types are therefore more likely to resemble a functional liver. Further studies based on multiple relevant cell types in co-culture may facilitate a better understanding of the effects at the tissue/organ level of oxLDL challenge.

To conclude, this *in vitro* study addressed the effects of mildly and heavily oxLDL on rat LSEC morphology and function. LSECs remain viable and functional as scavenger cells, though with detrimental effects on LSECs morphology including the loss of sieve plates and ruptured fenestrations and reduced degradation capacity for stabilin ligands. Thus, oxLDLs cause adverse effects on LSECs and are likely detrimental for LSEC function in maintaining circulatory homeostasis. It is therefore likely that excessive circulating oxLDL levels have the potential to exacerbate age-related endothelial thickening and defenestration (“pseudocapillarization”<sup>26,7</sup>) and reduction in waste degradation<sup>25</sup>. This would create a vicious cycle with

reduced LSEC-mediated LDL/oxLDL clearance, leading to increased levels of both substrates to further degrade LSEC function. Interventions that maintain circulating LDL at lower levels may therefore be of benefit for liver health.

## Materials and Methods

### Animals and ethics statements

Sprague Dawley male and female rats were obtained from Charles River Laboratories (Sulzfeld, Germany) and Janvier Labs (Le Genest-Saint-Isle, France). The rats were group-housed (2–3 rats/cage) in 135 G Euro-standard type IV conventional cages (Tecniplast, Italy) with aspen bedding (Scanbur, Norway) and with nesting material, rat tunnels and aspen chew blocks (Sizzelnest®, Datesand, UK) as environmental enrichment. The rats were kept under controlled environmental conditions (21 °C ± 1°, relative humidity 55% ± 5% and 12 h light/12 h dark cycle), at the specific pathogen free animal research facility at the University of Tromsø (UiT) – The Arctic University of Norway. The rats had free access to water and standard chow (RM1-E, Special Diet Service, UK). The experimental protocols and animal handling were approved by the National Animal Research Authority at the Norwegian Food Safety Authority (approval IDs: 8455 and 24732), and experiments were performed in compliance with the European Convention for the protection of Vertebrate Animals used for Experimental and Other Scientific Purposes. All animals were euthanized and died from exsanguination while in deep surgical anesthesia during the liver perfusion procedure (for anesthesia protocol see section “Rat LSEC isolation and cell culture”).

### Material

Collagenase was purchased from Worthington Biochemical Corporation (Lakewood, NJ, USA). Carrier-free Na<sup>125</sup>I from PerkinElmer Norge AS (Oslo, Norway). Bovine serum albumin (BSA) from MP Biomedicals (Solon, OH, USA). Human fibronectin was purified from human plasma by affinity chromatography on Gelatin Sepharose 4B as described by the manufacturer (GE Healthcare, Uppsala, Sweden). Percoll and PD-10 columns (Sephadex G-25) from GE Healthcare. Serum-free Roswell Park Memorial Institute (RPMI-1640) cell culture medium (supplemented with 0.006% penicillin, and 0.01% streptomycin). Culture dishes of 35 mm diameter and #1.5 glass coverslip-bottom were purchased from MatTek Corp. (Ashland, MA, USA). Trichloroacetic acid (TCA) from Merck (Darmstadt, Germany). Formaldehyde-treated bovine serum albumin (FSA) was prepared by treating BSA with 10% formaldehyde in 0.2 M carbonate buffer, pH 10, for 3 days as described by Mego et al.<sup>68</sup>. Ethylenediaminetetraacetic acid (EDTA) from Sigma Chemical Company (St. Louis, MO, USA). Human serum albumin (HSA) from Octapharma (Ziegelbrücke, Switzerland). Live cell imaging solution was from ThermoFisher (Oslo, Norway). CellMask™ Green and Orange was from Fisher Scientific (Cat. No. C37608 and C10045 Oslo, Norway). Lactate dehydrogenase (LDH)-Glo™ cytotoxicity assay was purchased from Promega (Nacka, Sweden). SE-1 antibody, anti-mouse IgG2a+b MACS® microbeads and necessary reagents for rat cell extraction were obtained from Miltenyi Biotec. Alexa Fluor™ 488 and 647 NHS Ester (Cat. Nr. A20000 and A20006) for coupling to FSA were ordered from ThermoFisher.

Antibodies for immunostaining of cells were bought from Santa Cruz (anti  $\alpha$ -tubulin AF488 and AF647, Cat. Nr. sc-23948) and Sigma-Aldrich (Phalloidin-Atto 647 N, Cat. Nr. 65906), as was DAPI dihydrochloride (Cat. Nr. D8417). The eNOS antibody (Cat. Nr. MA5-47674), the phosphorylated-eNOS antibody (PA5-104858), the donkey anti-mouse AlexaFluor 488 antibody (Cat. Nr. A21202), the donkey anti-rabbit AlexaFluor 555 antibody (Cat. Nr. A31573), ProLong glass anti-fade mounting medium (Cat. Nr. P36982) and Phalloidin Alexa Fluor 555 (Cat. Nr. A34055) were obtained from ThermoFisher. The KLF2 primer (Assay ID: Rn01420496\_gH) and eNOS primer (Assay ID: Rn07312037\_g1) (Cat. Nr. 4448892), the 2-Step Fast-Cells-to-CT Kit, 18 s rRNA conjugated to a VIC probe and the Griess Assay kit were purchased from ThermoFisher (Cat. Nr. G7921).

### Oxidation of LDL

LDL (density: 1.019–1.063 g/mL) was isolated from fresh human plasma by density gradient ultracentrifugation<sup>69</sup>, and preserved in 10% sucrose in 150 mM NaCl with 0.24 mM EDTA (pH 7.4 at –80 °C)<sup>70</sup>. Sucrose was removed by dialysis at 4 °C against phosphate-buffered saline (PBS) before further use. The protein concentration was determined by Nanodrop 2000 Spectrophotometer (Thermo Scientific, Oslo, Norway).

LDL was oxidized with CuSO<sub>4</sub> (1 mM) at 37 °C for 3 or 24 h to produce oxLDL<sub>3</sub> and oxLDL<sub>24</sub> (mildly and heavily oxidized LDL forms), respectively. The oxidation process was terminated by adding EDTA to a final concentration of 305 M after which samples were stored under nitrogen at 4 °C for ≤ 1 week before use to prevent further oxidation. Before use, CuSO<sub>4</sub> and EDTA were removed by extensive dialysis against PBS at 4 °C. Relative electrophoretic mobility (REM)<sup>71</sup> of differently oxLDLs was measured and compared with non-copper sulfate-treated LDL: oxLDL<sub>3</sub>: 1.42 ± 0.20 and oxLDL<sub>24</sub>: 1.79 ± 0.34; respectively, in 3–4 experiments (means ± SD).

### Rat LSEC isolation and cell culture

The rats (body weight 150–300 g) were anesthetized with a mixture (ZRF-mix) of zolazepam/tiletamine hydrochloride 12.9/12.9 mg/mL (Zoletil forte vet, Virbac, Norway), xylazine 1.8 mg/mL (Rompun, Bayer Nordic, Norway) and fentanyl 10.3 µg/mL (Actavis, Norway), injected intraperitoneally. LSECs were isolated and purified as described by Smedsrød, et al.<sup>72</sup> additionally using MACS magnetic microbeads. Briefly, after liver perfusion and digestion with Liberase™ (Roche), parenchymal cells were removed by differential centrifugation. LSECs were then separated by magnetic bead separation with anti-SE1 antibodies and anti-mouse IgG2a+b MACS® microbeads. For morphological analyses, the cells were plated on 0.2 mg/mL human fibronectin coated #1.5 coverslips (Sigma-Aldrich). The cells were cultured (37 °C, 5% CO<sub>2</sub>) for two to three hours in serum-free RPMI-1640. Fibronectin coating was performed with just enough volume to completely cover the surface area. After 10 min of incubation at room temperature (RT), the redundant fibronectin solution was rinsed with PBS and cells were then seeded. The LSECs were treated with mildly (3 h) or heavily (24 h) oxLDLs at 10, 40, or 80 µg/mL, doses were selected based on previous work<sup>26</sup> for 30 to 120 min to determine effects on fenestrations, then fixed with 4% formaldehyde (FA) in phosphate buffered saline (PBS) or PHEM buffer and 0.02 M sucrose (Sigma-Aldrich, Oslo, Norway), pH 7.2 for 15 min. Coverslips were kept in PBS/PHEM for later use. Some cells were incubated with FSA coupled to Alexa Fluor 488 or 647 (FSA-AF488/647) for 10–15 min before fixation.

### Structured illumination microscopy (SIM)

After fixation, the cells were stained with CellMask™ Green (5 µg/mL in serum-free RPMI) for 10 min, and immediately imaged using a commercial super-resolving SIM (DeltaVision/OMXv4.0 BLAZE, GE Healthcare) with a 60×1.42NA oil-immersion objective (Olympus). 3D-SIM images stacks of 1–2 µm were acquired with a z-distance of 125 nm and with 15 raw images per plane (five phases, three angles). Raw datasets were computationally reconstructed using SoftWoRx software (GE Healthcare). For live cell SIM, LSEC cultures were seeded in human fibronectin (0.2 mg/mL) coated MatTek dishes (35 mm Dish /No 1.5 coverslip, Ashland, MA, USA) with RPMI-1640 for 1 h at 37 °C. Unattached cells were gently washed away, and LSEC cultures were allowed an additional 1–2 h in culture to stretch their cytoplasm prior to imaging.

Fresh working solutions were prepared in a warm live cell imaging solution at 5 µg/mL of CellMask™ Green Plasma Membrane Stain. LSEC cultured dishes were placed on the pre-warmed 36 °C SIM holder. RPMI culture media was replaced with the aforementioned imaging solution, and after 5–10 min incubation, cells were imaged for 20 frames in 30 min.

### Light microscopy

The fixed cells on coverslips from storage were washed once with PBS/PHEM and permeabilized with 0.5% triton X in PBS for 2 min. After washing, specimens were incubated with  $\alpha$ -tubulin-AF488 or  $\alpha$ -tubulin-

AF647 (2 µg/mL in 1% PBS-T) overnight (ON) at RT. Four washes with PBS/PHEM followed: for 5 min, 10 min, 30 min and 1 hour. The cells were incubated with Phalloidin-Atto 647 N or Phalloidin Alexa Fluor 555 (2 µL in 100 µL PHEM for 90 min, prepared from recommended stock solution). After multiple washes, the samples were stained with CellMask™ orange or green (5 µg/mL), if not incubated with FSA-AF488/647, and DAPI (2 µg/mL) for 10 min. After two more washes with PHEM/PBS and one with water, the coverslips were mounted on microscope slides with a drop of ProLong™ Glass Antifade mountant. The samples were kept at 4 °C in the dark until imaging with EVOS M5000 using the DAPI, GFP, RFP and Cy5 light cubes or the Zeiss LSM 880 confocal microscope (C-Apochromat 40x water objective with a NA of 1.2).

### Scanning electron microscopy (SEM)

For SEM preparation, the treated specimens were fixed overnight in McDowell's fixative (4% formaldehyde (FA), 1% glutaraldehyde (GA), in phosphate buffer, pH 7.2). After washes with 0.1 M PHEM buffer, the coverslips containing the cells were treated with 1% tannic acid in 0.15 mol/l cacodylic buffer for 1 h, 1% OsO<sub>4</sub> in 0.1 mol/l cacodylic buffer for 1 h, dehydrated in ethanol (30%, 60%, 90% for 5 min each, 5 times 100% ethanol for 4 min), and incubated twice in hexamethyldisilazane (Sigma-Aldrich, Oslo, Norway) for 2 min each, dried, and sputter-coated with 10 nm gold/palladium alloys. Specimens were examined using a commercial SEM (Sigma HV0307, Zeiss), run at 2 kV. Large fields of view containing cells were randomly acquired in specific locations on the stubs to show cell culture condition and cell size, and high-resolution SEM images of a cell at magnification of 10-15 K were randomly acquired to observe fenestration alterations. Fenestrations were defined as open pores with diameters between 50 and 300 nm; gaps as open pores with a diameter larger than 300 nm.

### Endocytosis and degradation assay

For quantitative studies of endocytosis and degradation, fully confluent cultures of rat LSECs (approx. 0.25–0.30 × 10<sup>6</sup> cells/per well) established in 48-well culture dishes coated with human fibronectin, were treated with different oxLDL preparations (oxLDL<sub>3</sub> and oxLDL<sub>24</sub> at concentrations of 10, 40, 80 µg/mL with 1% HSA in RPMI culture media) for 30 min at 37 °C. Subsequently, 20,000 cpm <sup>125</sup>I-FSA in serum-free RPMI with HSA was added to each well and incubated for another two hours. Thereafter, the cell-associated and degraded FSA fractions were assayed according to Li et al.<sup>73</sup>. A Wilcoxon Signed-Rank test was performed in R to determine significant differences between the same treatments in male vs female cells. When no significance was detected, samples were combined and a paired two-tailed t-test was run with non-normalized values. Differences were considered significant if  $p < 0.05$ .

The LDH-Glo cytotoxicity assay was performed according to manufacturer's instructions, including freezing the samples in storage buffer before analyzing them another day. The luminescence was measured with the ClarioStar®Plus microplate reader after 30 and 60 min.

### Statistical analyses

Statistical analyses were conducted to assess the impact of oxLDL treatment on the endocytosis potential of LSECs. Difference between both male and female subjects was analyzed using Wilcoxon rank-sum test, to analyze if merging them would introduce significant bias. For variables showing no significant differences between sexes ( $p > 0.05$ ), normality was assessed using the Shapiro-Wilk test. Normality was assumed for p-values above 0.05. Variables meeting the normality criterion were subjected to paired T-tests to compare each treatment group with the control group (treated with RPMI). In cases where variables were non-normally distributed, the Wilcoxon signed-rank test was utilized, paired with the control group (RPMI). Visualization of the results was conducted using the ggplot package in R<sup>74</sup>.

### qPCR

Cell lysis and cDNA synthesis were performed using the 2-Step Fast-Cells-to-CT Kit following the manufacturer's protocols. qPCR was conducted

using TaqMan Fast Universal PCR mix. Target primers conjugated to a FAM probe were used to assess KLF2 and eNOS expression levels, while 18 s rRNA conjugated to a VIC probe served as the endogenous control. qPCR was run on a RealTime PCR LightCycler 96® system (Roche Life Sciences). Cycle threshold (CT) values were extracted and normalized to the endogenous control to account for cell number, followed by normalization to the control sample set using the  $\Delta\Delta CT$  method, presented as fold change to untreated control. Normality was assessed using Shapiro-Wilks test. Values were log transformed for better visualisation, significance was calculated if normality criterion was met, using One-Way ANOVA followed by Tukey's honestly significant difference test (Tukey's HSD). Statistical significance of treatment effects compared to control is indicated by asterisks (\*, \*\*, \*\*\*), where \* denotes  $p < 0.05$ , \*\*  $p < 0.01$ , and \*\*\*  $p < 0.001$ .

### Data availability

Data is provided within the manuscript or supplementary information files.

Received: 24 April 2024; Accepted: 25 September 2024;

Published online: 23 October 2024

### References

- Brown, M. S. & Goldstein, J. L. Receptor-mediated endocytosis: Insights from the lipoprotein receptor system. *Proc. Natl. Acad. Sci. USA*. **76**, 3330–3337 (1979).
- Faggiotto, A., Ross, R. & Harker, L. Studies of hypercholesterolemia in the nonhuman primate. I. Changes that lead to fatty streak formation. *Arteriosclerosis* **4**, 323–340 (1984).
- Faggiotto, A. & Ross, R. Studies of Hypercholesterolemia in the Nonhuman Primate II. Fatty Streak Conversion to Fibrous Plaque. *Arterioscler. Thromb. Vasc. Biol.* **4**, 341–356 (1984).
- Masuda, J. & Ross, R. Atherogenesis during low level hypercholesterolemia in the nonhuman primate: I. Fatty streak formation. *Arterioscler. Thromb. Vasc. Biol.* **10**, 164–177 (1990).
- Masuda, J. & Ross, R. Atherogenesis during low level hypercholesterolemia in the nonhuman primate: II. Fatty streak overversion to Fibrous Plaque. *Arterioscler. Thromb. Vasc. Biol.* **10**, 178–187 (1990).
- Goldstein, J. L., Ho, Y. K., Basu, S. K. & Brown, M. S. Binding site on macrophages that mediates uptake and degradation of acetylated low density lipoprotein, producing massive cholesterol deposition. *Proc. Natl. Acad. Sci. USA*. **76**, 333–337 (1979).
- Steinberg, D. The LDL modification hypothesis of atherogenesis: an update. *J. Lipid Res.* **50**, S376–S381 (2009).
- Steinberg, D. Low density lipoprotein oxidation and its pathobiological significance. *J. Biol. Chem.* **272**, 20963–20966 (1997).
- Rader, D. J. & Daugherty, A. Translating molecular discoveries into new therapies for atherosclerosis. *Nature* **451**, 904–913 (2008).
- Avogaro, P., Bon, G. B. & Gazzolato, G. Presence of a modified low density lipoprotein in humans. *Arteriosclerosis* **8**, 79–87 (1988).
- Ehara, S. et al. Elevated levels of oxidized low density lipoprotein show a positive relationship with the severity of acute coronary syndromes. *Circulation* **103**, 1955–1960 (2001).
- Holvoet, P., Stassen, J. M., Van Cleemput, J., Collen, D. & Vanhaecke, J. Oxidized low density lipoproteins in patients with transplant-associated coronary artery disease. *Arterioscler. Thromb. Vasc. Biol.* **18**, 100–107 (1998).
- Holvoet, P., Vanhaecke, J., Janssens, S., Van De Werf, F. & Collen, D. Oxidized LDL and malondialdehyde-modified LDL in patients with acute coronary syndromes and stable coronary artery disease. *Circulation* **98**, 1487–1494 (1998).
- Itabe, H. & Takano, T. Oxidized low density lipoprotein: the occurrence and metabolism in circulation and in foam cells. *J. Atheroscler. Thromb.* **7**, 123–131 (2000).
- Palinski, W. et al. Low density lipoprotein undergoes oxidative modification in vivo. *Proc. Natl. Acad. Sci. USA*. **86**, 1372–1376 (1989).

16. Jessup, W. & Kritharides, L. Metabolism of oxidized LDL by macrophages. *Curr. Opin. Lipidol.* **11**, 473–481 (2000).
17. Watson, A. D. et al. Structural identification by mass spectrometry of oxidized phospholipids in minimally oxidized low density lipoprotein that induce monocyte/endothelial interactions and evidence for their presence in vivo. *J. Biol. Chem.* **272**, 13597–13607 (1997).
18. Ahotupa, M. & Vasankari, T. J. Baseline diene conjugation in LDL lipids: An indicator of circulating oxidized LDL. *Free Radic. Biol. Med.* **27**, 1141–1150 (1999).
19. Berliner, J. A. et al. Minimally modified low density lipoprotein stimulates monocyte endothelial interactions. *J. Clin. Invest.* **85**, 1260–1266 (1990).
20. Glass, C. K. & Witztum, J. L. Atherosclerosis: The Road Ahead Review. *Cell* **104**, 503–516 (2001).
21. Schwartz, C. J., Valente, A. J., Sprague, E. A., Kelley, J. L. & Nerem, R. M. The Pathogenesis of Atherosclerosis: An Overview. *Clin. Cardiol.* **14**, 11–16 (1991).
22. Steinberg, D. et al. Modifications of low-density lipoprotein. *N. Engl. J. Med.* **320**, 915–924 (1989).
23. Witztum, J. L. & Steinberg, D. Role of oxidized low density lipoprotein in atherogenesis. *J. Clin. Invest.* **88**, 1785–1792 (1991).
24. Brinkley, T. E. et al. Plasma oxidized low-density lipoprotein levels and arterial stiffness in older adults the health, aging, and body composition study. *Hypertension* **53**, 846–852 (2009).
25. Simon-Santamaria, J. et al. Age-Related changes in scavenger receptor-mediated endocytosis in rat liver sinusoidal endothelial cells. *Journals Gerontol. - Ser. A Biol. Sci. Med. Sci.* **65 A**, 951–960 (2010).
26. Oteiza, A., Li, R., McCuskey, R. S., Smedsrød, B. & Sørensen, K. K. Effects of oxidized low-density lipoproteins on the hepatic microvasculature. *Am. J. Physiol. - Gastrointest. Liver Physiol.* **301**, 684–693 (2011).
27. Li, R. et al. Role of liver sinusoidal endothelial cells and stabilins in elimination of oxidized low-density lipoproteins. *Am. J. Physiol. - Gastrointest. Liver Physiol.* **300**, 71–81 (2011).
28. Man, J. J., Beckman, J. A. & Jaffe, I. Z. Sex as a Biological Variable in Atherosclerosis. *Circ. Res.* **126**, 1297–1319 (2020).
29. Wentzel, J. J. et al. Sex-related differences in plaque characteristics and endothelial shear stress related plaque-progression in human coronary arteries. *Atherosclerosis* **342**, 9–18 (2022).
30. Klein, S. L. & Flanagan, K. L. Sex differences in immune responses. *Nat. Rev. Immunol.* **16**, 626–638 (2016).
31. Fauchon, C. et al. Sex differences in brain modular organization in chronic pain. *Pain* **162**, 1188–1200 (2021).
32. Walker, C. J., Schroeder, M. E., Aguado, B. A., Anseth, K. S. & Leinwand, L. A. Matters of the heart: Cellular sex differences. *J. Mol. Cell. Cardiol.* **160**, 42–55 (2021).
33. European Commission. *Gendered Innovations*. <https://Op.Europa.Eu/En/Publication-Detail/-/Publication/33B4C99F-2E66-11Eb-B27B-01Aa75Ed71a1/Language-En> (2020). <https://doi.org/10.2777/53572>.
34. Arnegard, M. E., Whitten, L. A., Hunter, C. & Clayton, J. A. Sex as a Biological Variable: A 5-Year Progress Report and Call to Action. *J. Women's Heal.* **29**, 858–864 (2020).
35. Yla-Herttuala, S. et al. Evidence for the presence of oxidatively modified low density lipoprotein in atherosclerotic lesions of rabbit and man. *J. Clin. Invest.* **84**, 1086–1095 (1989).
36. Ling, W. et al. Oxidized or acetylated low density lipoproteins are rapidly cleared by the liver in mice with disruption of the scavenger receptor class A type I/II gene. *Journal of Clinical Investigation* **100**, 244–252 (1997).
37. Van Berkel, T. J. C., De Rijke, Y. B. & Kruijt, J. K. Different fate in vivo of oxidatively modified low density lipoprotein and acetylated low density lipoprotein in rats: Recognition by various scavenger receptors on Kupffer and endothelial liver cells. *J. Biol. Chem.* **266**, 2282–2289 (1991).
38. Itabe, H., Mori, M., Fujimoto, Y., Higashi, Y. & Takano, T. Minimally Modified LDL Is an Oxidized LDL Enriched with Oxidized Phosphatidylcholines. *J. Biochem.* **134**, 459–465 (2003).
39. Smedsrød, B. Clearance function of scavenger endothelial cells. *Comp. Hepatol.* **3**(Suppl 1), S22 (2004).
40. Fraser, R., Bosanquet, A. G. & Day, W. A. Filtration of chylomicrons by the liver may influence cholesterol metabolism and atherosclerosis. *Atherosclerosis* **29**, 113–123 (1978).
41. Fraser, R., Dobbs, B. R. & Rogers, G. W. T. Lipoproteins and the liver sieve: The role of the fenestrated sinusoidal endothelium in lipoprotein metabolism, atherosclerosis, and cirrhosis. *Hepatology* **21**, 863–874 (1995).
42. Fraser, R. et al. The liver sieve and atherosclerosis. *Pathology* **44**, 181–186 (2012).
43. Miyao, M. et al. Pivotal role of liver sinusoidal endothelial cells in NAFLD/NASH progression. *Lab. Investig.* **95**, 1130–1144 (2015).
44. Shetty, S., Lalor, P. F. & Adams, D. H. Liver sinusoidal endothelial cells – gatekeepers of hepatic immunity. *Nat. Rev. Gastroenterol. Hepatol.* **15**, 555–567 (2018).
45. Dabravolski, S. A. et al. The Role of KLF2 in the Regulation of Atherosclerosis Development and Potential Use of KLF2-Targeted Therapy. *Biomedicines* **10**, 254 (2022).
46. SenBanerjee, S. et al. KLF2 is a novel transcriptional regulator of endothelial proinflammatory activation. *J. Exp. Med.* **199**, 1305–1315 (2004).
47. Marrone, G. et al. KLF2 exerts antifibrotic and vasoprotective effects in cirrhotic rat livers: Behind the molecular mechanisms of statins. *Hepatology* **64**, 1434–1443 (2015).
48. Angolano, C. et al. A20/TNFAIP3 Increases ENOS Expression in an ERK5/KLF2-Dependent Manner to Support Endothelial Cell Health in the Face of Inflammation. *Front. Cardiovasc. Med.* **8**, 1–14 (2021).
49. Blomhoff, R. et al. Clearance of acetyl low density lipoprotein by rat liver endothelial cells. Implications for hepatic cholesterol metabolism. *J. Biol. Chem.* **259**, 8898–8903 (1984).
50. Elvevold, K. H., Nedredal, G. I., Revhaug, A. & Smedsrød, B. Scavenger properties of cultivated pig liver endothelial cells. *Comp. Hepatol.* **3**, 1–11 (2004).
51. Deleve, L. D. Liver sinusoidal endothelial cells in hepatic fibrosis. *Hepatology* **61**, 1740–1746 (2015).
52. Xie, G., Wang, L., Wang, X., Wang, L. & DeLeve, L. D. Isolation of periportal, midlobular, and centrilobular rat liver sinusoidal endothelial cells enables study of zoned drug toxicity. *Am. J. Physiol. - Gastrointestinal Liver Physiol.* **299** <https://doi.org/10.1152/ajpgi.00302.2010> (2010).
53. Maeso-Díaz, R. et al. Effects of aging on liver microcirculatory function and sinusoidal phenotype. *Aging Cell* **17**, 1–14 (2018).
54. Chang, Y. H., Abdalla, D. S. P. & Sevanian, A. Characterization of cholesterol oxidation products formed by oxidative modification of low density lipoprotein. *Free Radic. Biol. Med.* **23**, 202–214 (1997).
55. Oorni, K., Pentikainen, M. O., Ala-Korpela, M. & Kovanen, P. T. Aggregation, fusion, and vesicle formation of modified low density lipoprotein particles: Molecular mechanisms and effects on matrix interactions. *J. Lipid Res.* **41**, 1703–1714 (2000).
56. Vidal-Vanaclocha, F. & Barberá-Guillem, E. Fenestration patterns in endothelial cells of rat liver sinusoids. *J. Ultrastruct. Res. Mol. Struct. Res.* **90**, 115–123 (1985).
57. Wisse, E., de Zanger, R. B., Charels, K., van der Smissen, P. & McCuskey, R. S. The liver sieve: Considerations concerning the structure and function of endothelial fenestrae, the sinusoidal wall and the space of disse. *Hepatology* **5**, 683–692 (1985).
58. Crang, R. F. E. & Klomprens, K. L. Artifacts in Biological Electron Microscopy. *Science* **242**, 233 (1988).
59. Cogger, V. C. et al. Three-dimensional structured illumination microscopy of liver sinusoidal endothelial cell fenestrations. *J. Struct. Biol.* **171**, 382–388 (2010).

60. Bottomley, A. L., Turnbull, L., Whitchurch, C. B. & Harry, E. J. Immobilization techniques of bacteria for live super-resolution imaging using structured illumination microscopy. *Methods Mol. Biol.* **1535** 197–209 [https://doi.org/10.1007/978-1-4939-6673-8\\_12](https://doi.org/10.1007/978-1-4939-6673-8_12) (2017).
61. Schwartz, T. et al. Direct fluorescent-dye labeling of  $\alpha$ -tubulin in mammalian cells for live cell and superresolution imaging. *Mol. Biol. Cell* **28**, 2747–2756 (2017). at.
62. Guixé-Muntet, S. et al. Nuclear deformation mediates liver cell mechanosensing in cirrhosis. *JHEP Rep.* **2**, 100145 (2020).
63. De Rijke, Y. B., Biessen, E. A. L., Vogelesang, C. J. M. & Van Berkel, T. J. C. Binding characteristics of scavenger receptors on liver endothelial and Kupffer cells for modified low-density lipoproteins. *Biochem. J.* **304**, 69–73 (1994).
64. Falkowska-Hansen, B., Falkowski, M., Metharom, P., Kronic, D. & Goerdts, S. Clathrin-coated vesicles form a unique net-like structure in liver sinusoidal endothelial cells by assembling along undisrupted microtubules. *Exp. Cell Res.* **313**, 1745–1757 (2007).
65. Mönkemöller, V., Øie, C., Hübner, W., Huser, T. & McCourt, P. Multimodal super-resolution optical microscopy visualizes the close connection between membrane and the cytoskeleton in liver sinusoidal endothelial cell fenestrations. *Sci. Rep.* **5**, 1–10 (2015).
66. Li, W., Yuan, X. M., Olsson, A. G. & Brunk, U. T. Uptake of oxidized LDL by macrophages results in partial lysosomal enzyme inactivation and relocation. *Arterioscler. Thromb. Vasc. Biol.* **18**, 177–184 (1998).
67. Le Couteur, D. G., Fraser, R., Cogger, V. C. & McLean, A. J. Hepatic pseudocapillarisation and atherosclerosis in ageing. *Lancet* **359**, 1612–1615 (2002).
68. Mego, J. L., Bertini, F. & McQueen, J. D. The use of formaldehyde-treated 131-I-albumin in the study of digestive vacuoles and some properties of these particles from mouse liver. *J. Cell Biol.* **32**, 699–707 (1967).
69. Redgrave, T. G., Roberts, D. C. K. & West, C. E. Separation of Plasma Lipoproteins by density-gradient ultracentrifugation. *Anal. Biochem.* **65**, 42–49 (1975).
70. Rumsey, S. C., Galeano, N. F., Arad, Y. & Deckelbaum, R. J. Cryopreservation with sucrose maintains normal physical and biological properties of human plasma low density lipoproteins. *J. Lipid Res.* **33**, 1551–1561 (1992).
71. Noble, R. P. Electrophoretic separation of plasma lipoproteins in agarose gel. *J. Lipid Res.* **9**, 693–700 (1968).
72. Smedsrød, B. & Pertoft, H. Preparation of pure hepatocytes and reticuloendothelial cells in high yield from a single rat liver by means of Percoll centrifugation and selective adherence. *J. Leukoc. Biol.* **38**, 213–230 (1985).
73. Li, R. et al. Endocytosis of advanced glycation end-products in bovine choriocapillaris endothelial cells. *Microcirculation* **16**, 640–655 (2009).
74. Wickham, H. Data Analysis. in *ggplot2: Elegant Graphics for Data Analysis* (eds. Gentleman, R., Hornik, K. & Parmigiani, G.) 189–201 (Springer Nature, 2016).

## Acknowledgements

This study was supported by grants from the Tromsø Research Foundation/ Trond Mohn, the University of Tromsø-The Arctic University of Norway, the Research Council of Norway FRIMED no. 325446 (Project PACA-Pill) and no. 275241 (Project Sugar Crush), Marie Skłodowska-Curie Grant

Agreement No. 766181 (Project DeLIVER) and Horizon Europe EIC Pathfinder Open Grant Nr. 101046928 (Project DeLIVERy). The funders have not played a role in the research. We acknowledge Prof. Karen Kristine Sørensen's critical review of this manuscript. We would like to thank Dr. Karolina Szafranska, Tetyana Voloshyna, Dr. Ingelin Kyrrestad, Dr. Anett Larsen and Dr. Christopher Holte for the help with the production of cells, LDL and for the labeling of the radioactive FSA. We would also like to thank Mateusz Sar for the help with cell staining and EVOS microscopy and Gianina Dumitriu for the help with the Griess assay. Additionally, we would like to thank Randi Olsen, Tom-Ivar Eilertsen, Kenneth Bowitz Larsen and Dr. Anthimi Palara from the Advanced Microscopy Core Facility at UiT for their help with sample preparation and imaging with scanning electron microscopy and confocal microscopy.

## Author contributions

P.M. was responsible for study conception and design. Data was collected by H.M.; L.D.K.; A.O.; R.L.; D.L.W.; P.M.; W.H. and J.S. Analysis and interpretation of results was performed by H.M.; L.D.K.; A.O.; R.L.; E.C.S.; J.S.; W.H.; V.C.C.; D.L.C.; D.L.W.; T.H.; B.S.A.; C.Ø.; and P.M. Statistical analysis was performed by E.C.S. Draft manuscript preparation was by H.M.; L.D.K.; and P.M. Funding was secured by P.M.; V.C.C.; D.L.C.; and C.Ø. All authors reviewed the results and approved the final version of the manuscript.

## Competing interests

The authors declare no competing interests.

## Additional information

**Supplementary information** The online version contains supplementary material available at <https://doi.org/10.1038/s44355-024-00009-5>.

**Correspondence** and requests for materials should be addressed to Peter A. G. McCourt.

**Reprints and permissions information** is available at <http://www.nature.com/reprints>

**Publisher's note** Springer Nature remains neutral with regard to jurisdictional claims in published maps and institutional affiliations.

**Open Access** This article is licensed under a Creative Commons Attribution 4.0 International License, which permits use, sharing, adaptation, distribution and reproduction in any medium or format, as long as you give appropriate credit to the original author(s) and the source, provide a link to the Creative Commons licence, and indicate if changes were made. The images or other third party material in this article are included in the article's Creative Commons licence, unless indicated otherwise in a credit line to the material. If material is not included in the article's Creative Commons licence and your intended use is not permitted by statutory regulation or exceeds the permitted use, you will need to obtain permission directly from the copyright holder. To view a copy of this licence, visit <http://creativecommons.org/licenses/by/4.0/>.

© The Author(s) 2024